Theoretical study of the electronic spectrum of antimony oxide employing relativistic effective core potentials

Aleksey B. Alekseyev, HeinzPeter Liebermann, Robert J. Buenker, and Gerhard Hirsch

Citation: The Journal of Chemical Physics **102**, 2539 (1995); doi: 10.1063/1.468683
View online: http://dx.doi.org/10.1063/1.468683
View Table of Contents: http://scitation.aip.org/content/aip/journal/jcp/102/6?ver=pdfcov
Published by the AIP Publishing

Theoretical study of the electronic spectrum of antimony oxide employing relativistic effective core potentials

Aleksey B. Alekseyev,[a] Heinz-Peter Liebermann, Robert J. Buenker, and Gerhard Hirsch
Bergische Universität-Gesamthochschule Wuppertal, Fachbereich 9-Theoretische Chemie, Gaussstr. 20, D-42097 Wuppertal, Germany

(Received 12 September 1994; accepted 1 November 1994)

Potential energy curves and electric dipole transition moments between different electronic states are computed for the antimony oxide molecule employing a relativistic configuration interaction scheme including the spin–orbit coupling interaction. Comparison is made with available experimental data as well as with the corresponding results which were recently reported for the isovalent BiO. A full core relativistic effective core potential proves to be quite effective in describing the antimony inner shells, thereby reducing the amount of computations considerably relative to an all-electron CI treatment. The calculated bond lengths r_e for the $X_1\ ^2\Pi_{1/2}$ ground state and $C\ ^2\Sigma^-_{1/2}$ excited state agree to within 0.01 Å of the respective measured values and good agreement is also found for the vibrational frequencies ω_e of a large number of SbO states. The theoretical treatment tends to underestimate transition energy T_e values, typically by 1000–2000 cm^{-1}, reflecting the fact that all excited states have more open shells in their leading configurations than does the ground state itself. On the basis of the present calculations it has been possible to confirm a number of earlier assignments for the SbO upper states and also to aid in the experimental detection of several new transitions involving various $a\ ^4\Pi$ and $b\ ^4\Sigma^-$ species which were not known at the time this work was begun. Theoretical values for the radiative lifetimes of the $v'=0$ levels of each of the above electronic states have also been obtained, and they are found to agree within at least a factor of 2 in most cases with the recent experimental values obtained by Fink, Shestakov, and co-workers. The lone exception found to date is for the $B\ ^2\Sigma^+$ state, but it is noted that nonadiabatic interactions between it and the $b_1\ ^4\Sigma^-_{1/2}$ state, as already discussed in an earlier review by Rai and Rai, could be at least partially responsible for this result. © *1995 American Institute of Physics.*

I. INTRODUCTION

The electronic structure and spectroscopic characteristics of the group VA diatomic oxides has been a subject of great interest because it affords the opportunity of studying the role of relativistic effects over a large range of atomic number in a quite systematic manner for relatively simple yet chemically stable substances.[1] Standard MO theory predicts correctly that the ground states of all these molecules from NO to BiO possess a $...\sigma^2\pi^4\pi^*$ electronic configuration and that their lowest-lying excited states arise from $\pi\rightarrow\pi^*$, $\sigma\rightarrow\pi^*$, $\pi\rightarrow\sigma^*$, and $\pi^*\rightarrow\sigma^*$ transitions therefrom. As the electronegativity of the group VA atom in the series varies, there are only moderate changes in the shapes and relative positions of the corresponding λ-*s* potential curves which are obtained theoretically without consideration of spin-dependent forces. The role of spin–orbit coupling in determining the appearance of the potential energy curves at a more acceptable level of theory is quite decisive, however, particularly when attention is turned to the compounds of the heavier elements, antimony and bismuth. For example, the $X\ ^2\Pi$ zero-field splitting increases to 2272 cm^{-1} for SbO and reaches a value of 7089 cm^{-1} for BiO.

Until recently *ab initio* configuration interaction (CI) calculations which are of sufficient accuracy to help clarify the complex electronic structure of systems containing such heavy elements were impossible to carry out. The advent of relativistic effective core potentials (RECP's) (Refs. 2–5) which reduce the effect of the inner shells of heavy atoms to one-particle interactions, including spin-dependent properties, has changed this state of affairs dramatically, however. In the present laboratory a multireference CI package has been extended to accommodate these developments,[6] and one of the first applications carried out with it was for the BiO molecule.[7] In the present work attention will be given to the next lighter member of this series, SbO.

The first bands in the visible region of the spectrum of antimony oxide were reported by Mukherjee,[8] and work was continued over the next 40 years.[9–14] Seven distinct electronic transitions were identified in the process, all of which involve the $X\ ^2\Pi$ ground state.[15] Later Balfour and Ram[16,17] reinvestigated the $A\rightarrow X$ and $C\rightarrow X$ transitions and detected a new $H\rightarrow X$ system as well. These authors have also given a concise summary of previous experimental findings.[17] In addition to the $X\ ^2\Pi$ and $A\ ^2\Pi$ states, at least five other higher-lying species with T_e values relative to the ground state ranging from 26 594 cm^{-1} ($B\ ^2\Sigma$) to 39 785 cm^{-1} ($E\ ^2\Sigma$) were characterized quantitatively.[15,17] More recently high-resolution experiments have been carried out for this system by Fink, Shestakov, and co-workers[18] during the same time period in which the present CI calculations were being carried out. These new observations not only provided more precise information about the energy locations of the

[a]Fellow of the Alexander von Humboldt Foundation; on leave from the Institute of Physics, St. Petersburg State University, St. Petersburg, Russia.

 0021-9606/95/102(6)/2539/12/$6.00

previously known spectral bands, but also supplied quantitative information about the intensities of these features. These authors were also successful in finding new electronic transitions which had previously been overlooked in the spectral region under discussion. In the present study it will be demonstrated that there are actually 21 electronic states in SbO with T_e values lying at or below 35 000 cm^{-1}.

II. THEORETICAL APPROACH

The full-core RECP of Ross *et al.*[19] is employed to describe the antimony inner-shell electrons, so that only the $5s$ and $5p$ valence electrons are treated explicitly in the SCF and CI calculations. The AO basis chosen is the $3s3p$ primitive set recommended in the original reference[19] for use with this RECP, i.e., a basis set of triple-zeta-plus-polarization (TZP) quality after the inclusion of an additional d function with optimized exponent of 0.22 a_0^{-2}.[20] The $1s$ electrons of oxygen are also described by a core potential,[21] just as in the previous BiO theoretical treatment.[7] The corresponding AO basis is $[4s4p1d]$, also in uncontracted form.[7,21] The spin-independent part of the RECP's is employed in the λ-s SCF and CI calculations. Also as in the BiO work,[7] the SCF-MO's of the SbO^+ $^1\Sigma^+$ closed-shell ground state are employed as one-electron basis for the configuration interaction treatment. Experience[22] has shown that the corresponding virtual orbitals can be used effectively to describe the exclusively valence excited states which play a role in the low-energy spectrum of this molecule. The calculations are carried out formally in the C_{2v} subgroup, but the resulting MO's do transform as irreducible representations of the full $C_{\infty v}$ linear point group, a characteristic which is very desirable in the later stages of the theoretical treatment when the total symmetries of the eigenstates need to be identified.

The standard multireference single- and double-excitation CI method is employed (MRD-CI) (Ref. 23) throughout to obtain the λ-s electronic energies, wave functions, and properties. This technique makes use of configuration selection and perturbative energy extrapolation techniques[23] and employs the table CI algorithm[24] for efficient handling of the various open-shell cases which arise. A selection threshold of $T=1.0\times10^{-5}\ E_h$ is employed throughout, but some tests have been made for $T=5.0\times10^{-6}\ E_h$ to verify that a suitable level of convergence has been achieved in the standard treatment. Information about technical details of the MRD-CI calculations is given in Table I. Generally four to seven roots of a given λ-s symmetry are treated in each case, with generated secular equation orders falling in excess of one million. The corresponding selected CI spaces for which variational calculations are carried out have orders in the 5 000–15 000 range. The $C_{\infty v}$ notation for the most stable of the resulting eigenstates are also listed in Table I, along with the sums of the c^2 values for members of the reference set in each case. The latter values fall uniformly in the 92%–94% range, which is an indication that the various reference sets have been chosen with sufficient care for the purposes at hand.

Results are obtained for a series of bond distance values in the 2.8–8.0 a_0 range, in steps of 0.1 a_0 up to 4.1 a_0, followed by a step-size of 0.25 a_0 up to 5.5 a_0 and finally 0.5 a_0 for still longer bond distances. The reference configurations have been chosen on the basis of results obtained at a series of representative bond distances and are thereupon taken to be the same throughout the final series of λ-s calculations so as to ensure a balanced theoretical treatment over the entire range of internuclear separation. In particular, it is found to be especially important to include configurations which are dominant at large R values to accurately describe the bonding process at intermediate bond separations. Finally, the multireference analogue of the Davidson correction[25,26] is applied to the computed energy eigenvalues in order to estimate the effect of still higher excitations on the final results. Properties such as the electric dipole matrix elements between various pairs of electronic states are obtained using the variational wave functions themselves, without further correction.

TABLE I. Technical details of the MRD-CI calculations.[a]

C_{2v} sym.	N_{ref}/N_{root}	SAFTOT/SAFSEL	$C_{\infty v}$ notation	Σc_p^2
$^2B_{1,2}$	43/5	755 694/9 678	$1\ ^2\Pi$	0.9214
			$2\ ^2\Pi$	0.9216
			$1\ ^2\Phi$	0.9241
$^2A_1$	82/7	1 699 293/13 463	$1\ ^2\Sigma^+$	0.9203
			$1\ ^2\Delta$	0.9161
$^2A_2$	59/6	998 253/9 235	$1\ ^2\Sigma^-$	0.9192
			$1\ ^2\Delta$	0.9170
$^4B_{1,2}$	64/4	1 254 022/11 826	$1\ ^4\Pi$	0.9332
			$2\ ^4\Pi$	0.9148
$^4A_1$	70/5	2 004 876/15 440	$1\ ^4\Sigma^+$	0.9234
			$1\ ^4\Delta$	0.9262
$^4A_2$	76/4	1 222 564/10 822	$1\ ^4\Sigma^-$	0.9251
			$1\ ^4\Delta$	0.9252
$^6A_1$	29/2	825 309/6 266	$1\ ^6\Sigma^+$	0.9399
$^6B_{1,2}$	19/2	368 915/5 762	$1\ ^6\Pi$	0.9168

[a]The number of selected SAF's and the Σc_p^2 values over reference configurations (for the lowest roots of each symmetry) are given for $r=3.5\ a_0$. SAFTOT designates the total number of generated. SAFSEL the number of selected SAF's, N_{ref} and N_{root} refer to the number of reference configurations and roots treated, respectively.

The spin–orbit interaction is also included via RECP's. The calculations are carried out in the C_{2v} double group, with one degenerate irreducible representation for this odd-electron system. More details of the corresponding relativistic CI procedure may be found in the previous study of the BiO spectrum.[7] Rather than solve relatively large secular equations based on the combined CSF's from the various λ-s CI spaces, it is preferable in the present work to take the corresponding eigenfunctions as basis for much smaller diagonalizations. In this way the perturbative corrections described above[23,25,26] can be applied conveniently to the diagonal elements of the corresponding CI matrix. Test calculations with both methods have demonstrated that essentially equivalent results ensue from these two procedures, whereby the version favored in this work involves significantly less expenditure of computational resources. It might be thought that the use of λ-s eigenfunctions as a basis for a

subsequent relativistic CI would be less effective because of its failure to treat the spin-independent and spin-dependent interactions on equal footing, but such a position overlooks the fact that, at least for diatomics and other relatively symmetric systems, no spin–orbit matrix elements occur between functions of the same λ-*s* symmetry. This fact tends to make the λ-*s* eigenfunctions a natural basis for such a relativistic CI, as corroborated by overlap tests between the spin–orbit CI eigenfunctions in the combined CSF basis with the λ-*s* states themselves.

The Wigner–Eckart theorem is used to good effect in evaluating the necessary spin–orbit matrix elements between different M_s components of the various λ-*s* eigenstates. In practice two orthogonal basis sets are formed which correspond to the two degenerate components of the C_{2v} double group odd-electron irreducible representation. In one case the $M_s=1/2$ $^2A_1$ and $^2A_2$ species are combined with the corresponding $M_s=-1/2$ $^2B_1$ and $^2B_2$ functions, for example, whereas the opposite choices are made for the other basis. The resulting pair of secular equations lead to identical energy results, but to mutually orthogonal sets of eigenfunctions which are then employed in the computation of perpendicular components of the transition moment.

The final stage of the calculations begins with the fitting of the relativistic CI potential curves to polynomials which are employed to construct the appropriate Born–Oppenheimer nuclear motion Schrödinger equations, which are then solved numerically by means of the Numerov–Cooley method.[27] The corresponding electric dipole matrix elements between pairs of λ-*s* eigenfunctions are transformed over the relativistic CI eigenfunctions, and these results are also fitted to polynomials and averaged over various pairs of vibrational functions obtained above. The latter results are then employed to compute Einstein spontaneous emission coefficients for various vibrational transitions, generally involving either the $X_1\,^2\Pi_{1/2}$ or $X_2\,^2\Pi_{3/2}$ electronic states. The radiative lifetimes of a given upper vibrational state are obtained by summing over its Einstein coefficients with all lower-lying levels and inverting.

III. COMPUTED RELATIVISTIC CI POTENTIAL CURVES AND ELECTRONIC WAVE FUNCTIONS

A. Spin-independent results

The SbO λ-*s* potential curves obtained with interactions other than spin–orbit coupling are shown in Fig. 1. There is a rather close similarity between the antimony and bismuth oxide results of this genre (see Fig. 1 of Ref. 7). The ground state is the $...\sigma^2\pi^4\pi^*$ $X\,^2\Pi$ and the lowest excited states are generated by $\pi\rightarrow\pi^*$, $\sigma\rightarrow\pi^*$, and $\pi\rightarrow\sigma^*$ excitations. The first λ-*s* excited state is the $\pi\rightarrow\pi^*$ $^4\Pi$, but it occurs about 4000 cm^{-1} higher in SbO than in BiO, reflecting a general trend toward more compact energy level diagrams in heavier systems. One distinction in the results for these two oxides lies in the fact that the equilibrium bond distances r_e for the $\pi\rightarrow\pi^*$ states are notably larger in SbO than for the corresponding $\sigma\rightarrow\pi^*$ species, whereas there is virtually no difference between the analogous quantities in the bismuth counterpart.[7] All these excited state r_e values are larger than the respective ground state result because of the fact that electrons are being transferred from bonding to antibonding orbitals in each case. The results indicate, however, that in SbO the σ MO is not as strongly bonding as the π, unlike the situation in the heavier oxide. In general it should be noted that the antimony atom is more electronegative than its heavier group member, and hence there is significantly more mixing between Sb and O atomic orbitals in forming the above MO's than is the case for the analogous BiO species. Such orbital mixing tends to favor stronger bonds and weaker antibonds, in agreement with what has been calculated.

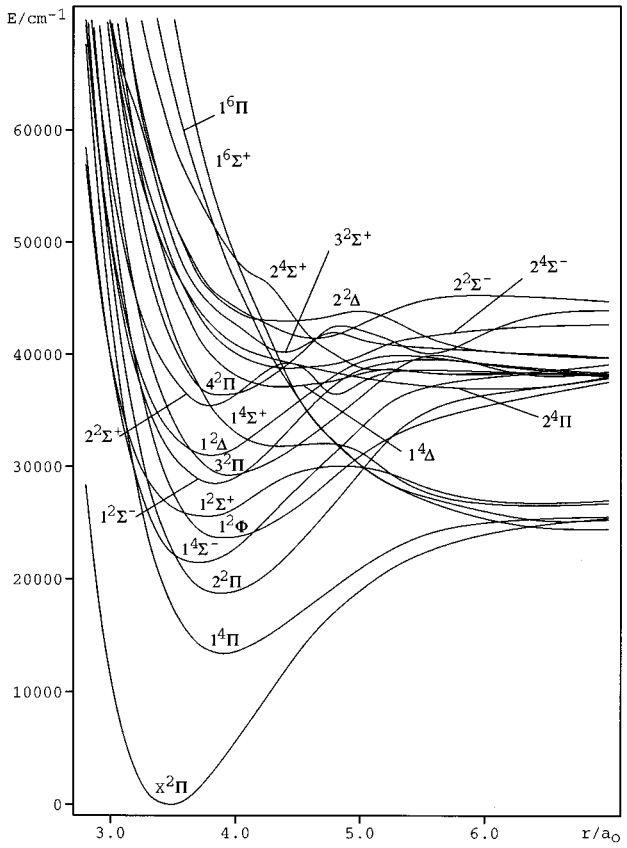

FIG. 1. Computed potential energy curves for the lowest-lying λ-*s* states of the SbO molecule obtained in a theoretical treatment without the inclusion of the spin–orbit interaction.

Both SbO and BiO have ground state atomic limits consisting of a nitrogenlike ^4S_u and $O(^3P_g)$, corresponding to five open-shell electrons in each case. Since the equilibrium configurations for both ground and low-lying excited states contain from one to three open-shell electrons, it is clearly necessary for avoided crossings to occur in the associated potential curves in passing from the bottoms of their wells to the separated-atoms limit. As a result the lowest $^2\Sigma^+$ state has a fairly large recombination barrier (Fig. 1). Similarly the lowest $^4\Sigma^+$ exhibits a broad shoulder in its potential curve in the 4.5–5.0 a_0 range of internuclear distance. There are no bound sextet states, so the corresponding $^6\Pi$ and $^6\Sigma^+$ states simply possess repulsive potential curves. The curve crossings for the lowest $^2\Pi$ and $^4\Pi$ occur at fairly large r values

and are thus not as evident in the figure as those for the Σ^+ states of the same multiplicity. All six of the above states should have exactly the same energy at the dissociation limit. Since the calculations are not carried out at the full CI limit, this result is only approximate in the present work. The observed deviations from this ideal are on the order of 1000–2000 cm^{-1} in the case of the lowest atomic limit, which results should be a good indication of the overall accuracy of the theoretical treatment employed throughout this study.

The $\pi \rightarrow \pi^*$ excitation produces the $^4\Pi$ state, followed by a $^2\Pi$, a $^2\Phi$, and then two more $^2\Pi$ species, exactly as in BiO (Fig. 1). The $^4\Sigma^-$ lying between 2 $^2\Pi$ and $^2\Phi$ comes from the $\sigma \rightarrow \pi^*$ excitation but the $^2\Sigma^+$ lying just above it is predominantly $\pi^* \rightarrow \sigma^*$ in character [related to the *K* state in BiO (Ref. 7)]. The other $\sigma \rightarrow \pi^*$ states occur in the order $^2\Sigma^- < ^2\Delta < 2\ ^2\Sigma^+$, consistent with the fact that the π^{*2} occupation leads to the order $^3\Sigma^- < ^1\Delta < ^1\Sigma^+$, from which $^{4,2}\Sigma^-$, $^2\Delta$, and $^2\Sigma^+$ states are generated upon coupling with the σ electron. Finally, as in BiO, a number of low-lying $\pi \rightarrow \sigma^*$ excited states are also present in the SbO λ-*s* spectrum (Fig. 1).

B. Relativistic CI with spin–orbit coupling

In the next stage of the calculations a number of λ-*s* eigenfunctions is selected as basis for a CI treatment including the spin–orbit coupling interaction as described by the relativistic effective core potentials (RECP's). Tests with the other standard approach in which the selected CSF sets from the various λ-*s* spaces are employed as basis for a Hamiltonian matrix representation have indicated that the former approach is quite effective. The treatment with the CSF basis involves solution of much larger secular equations than in the present calculations, but it has been found in numerous test cases that the resulting eigenfunctions overlap to a very high degree with the first few λ-*s* eigenfunctions of each symmetry (typically Σc_i^2 values of 98%–99% are obtained with only 10–20 λ-*s* species). In the present study, as for the BiO calculations,[7] a 37×37 secular equation has been solved at each *r* value. The lowest-lying five λ-*s* eigenstates of $^2B_1$, $^2B_2$ (four $^2\Pi$ and one $^2\Phi$) and $^2A_1$ (three $^2\Sigma^+$ and two $^2\Delta$) plus four $^2A_2$ species (two $^2\Sigma^-$ and two $^2\Delta$) have been chosen for this purpose, along with two $^4B_1$, $^4B_2$ ($^4\Pi$) and $^4A_1$ ($^4\Sigma^+$, $^4\Delta$) and three $^4A_2$ (two $^4\Sigma^-$ and $^4\Delta$) species (in the case of the quartets the number of basis functions must be multiplied by 2 to account for the various M_s values). More details of the treatment of the double group symmetry in these odd-electron CI calculations may be found in the BiO paper.[7] Two separate secular equations are solved in each case corresponding to the two partners in each degenerate double group representation. Some additional tests have been carried out at various bond distances with additional λ-*s* basis functions, but the indication is that a high level of convergence has been obtained with the treatment employing 37 such functions.

The resulting potential energy curves for the SbO molecule are shown in Fig. 2. The effect of the spin–orbit coupling is naturally less protracted than for the bismuth compound, but it is still quite significant. A good measure for this comparison is the $X_2 - X_1$ ground state splitting, which is less

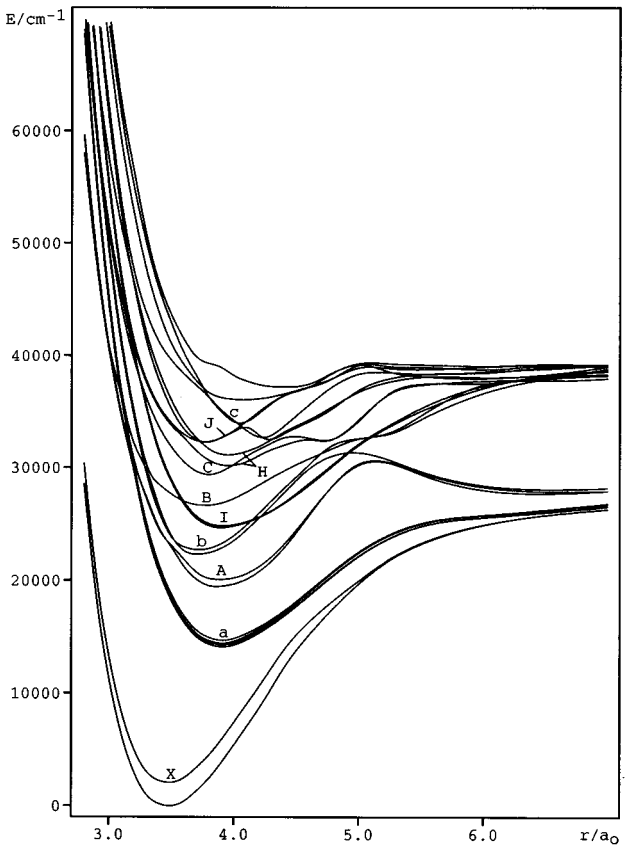

FIG. 2. Computed potential energy curves for the lowest-lying electronic states of the SbO molecule in the present theoretical treatment including spin–orbit coupling.

than one-third as much in SbO according to the experimental findings[15] (2272 cm^{-1} for SbO vs 7089 cm^{-1} in BiO). The strongly avoided crossing between the $\Omega = 3/2$ states arising from the $X\ ^2\Pi$ and $a\ ^4\Pi$ λ-*s* species in BiO is effectively absent in antimony oxide. More generally, from a comparison with Fig. 1 it is easily possible to recognize the dominant λ-*s* character in the spin-perturbed potential energy curve data in Fig. 2. For example, after the $X_1 - X_2$ pair the next four lowest-energy states derive almost exclusively from $a\ ^4\Pi$, as can be judged from the results in Tables II–III for the values of the squares of coefficients for the λ-*s* eigenfunctions in the various spin–orbit CI expansions, as well as from the potential curves themselves. The *A* states are predominantly $2\ ^2\Pi$ in character at small *r* values, but there are pronounced barriers in the neighborhood of $r = 5.0\ a_0$ which are caused by the spin–orbit mixing.

It should be noted that there is a change in nomenclature relative to that employed to describe the BiO spectrum. Because of the dominance of the λ-*s* character in the SbO states, it is convenient to distinguish between states of doublet multiplicity (with capital letters) and all others. Hence the $^4\Pi$ species are designated with a_i, $i = 1$–4 for the four related Ω values, while the two $^2\Pi$ states are labeled A_i. In BiO, by contrast, no distinction is made on the basis of spin multiplicity because the spin–orbit effects are much more pronounced. Hence, the analogous states for this system are

TABLE II. Composition of the lowest ten $\Omega=1/2$ states of SbO (c^2, %) at various bond distances r (in a_0).[a]

State	r	$1\,^2\Pi$	$2\,^2\Pi$	$3\,^2\Pi$	$4\,^2\Pi$	$1\,^4\Pi$	$2\,^4\Pi$	$1\,^4\Sigma^-$	$2\,^4\Sigma^-$	$1\,^2\Sigma^+$	$2\,^2\Sigma^+$	$3\,^2\Sigma^+$	$1\,^2\Sigma^-$	$2\,^2\Sigma^-$	$1\,^4\Sigma^+$	$2\,^4\Sigma^+$	$1\,^4\Delta$
$X_1\,^2\Pi_{1/2}$	3.0	99.7															
	3.5	99.4															
	4.0	98.7															
	5.0	97.6															
	6.0	96.3															
	6.5	91.4				7.0											
	7.0	89.5			1.0	8.7											
$a_2\,^4\Pi_{1/2}$	2.8									99.4							
	3.0					1.8		93.7		2.9	1.2						
	3.5			1.1		96.8											
	4.0			1.3		96.7											
	5.0			2.0		96.2											
	6.0				1.0	96.5											
	6.5					98.3											
$a_4\,^4\Pi_{1/2}$	2.8							98.0			1.0						
	3.0							2.9		96.7							
	3.5					99.2											
	4.0					99.5											
	5.0					99.2											
	6.0	1.7				97.8											
	6.5	7.8				92.0											
$A_2\,^2\Pi_{1/2}$	2.8		1.1			92.5							5.2				
	3.0		1.3			96.4											
	3.5		9.5					87.9			1.6						
	3.9		97.3	1.0													
	5.0		78.6							17.0					2.6		
	5.25		2.3							65.5					31.5		
	6.0														99.8		
	6.5														99.3		
$b_1\,^4\Sigma^-_{1/2}$	2.8					93.2							5.8				
	3.0					98.4											
	3.5		88.6	1.0				9.0									
	3.7		2.3					94.3			2.2						
	4.6							94.7				2.9					
	5.0		16.8							80.4					1.7		
	6.0									99.9							
	6.5									99.9							
$B\,^2\Sigma^+_{1/2}$	2.8					11.1					3.8		84.2				
	3.0		96.9			1.0							1.0				
	3.5									99.0							
	3.7									98.6							
	4.6						1.6		1.3	95.4							
	5.0		4.2												93.3		
	6.0		99.5														
	6.5		1.2		5.7		83.8										4.8
$C\,^2\Sigma^-_{1/2}$	2.8		97.1			1.3											
	3.0										4.0		93.9				
	3.5										3.6		95.4				
	3.8										3.5		94.5				
	4.1			2.8	1.7						3.7		89.5				
	4.25			15.3	1.9						3.3		67.1		8.6		
	4.4			46.9		2.0			1.4				1.3	1.0	43.6		
	4.75			1.0											96.3		
	5.0			1.3				94.4								1.8	
	5.5			11.3	5.4		35.8	29.7								13.0	
	6.0			44.5	5.5		35.7	2.9							7.2		
	6.5		57.3	7.8			32.6										
$H_2\,^2\Pi_{1/2}$	2.8							1.0			93.5		4.5				
	3.0			1.9				1.2			92.4		4.2				
	3.5			95.1		1.5					1.3						
	3.9			94.6		1.8											
	4.25			61.2		1.5							24.2		8.7		2.1
	5.0			58.1		1.9	2.9				2.5					1.6	27.3
	5.5					46.0		42.5			1.9						5.4
	6.0						91.2		4.6					1.2			
	6.5		31.9				66.4										

TABLE II. (*Continued*.)

State	r	$1\,^2\Pi$	$2\,^2\Pi$	$3\,^2\Pi$	$4\,^2\Pi$	$1\,^4\Pi$	$2\,^4\Pi$	$1\,^4\Sigma^-$	$2\,^4\Sigma^-$	$1\,^2\Sigma^+$	$2\,^2\Sigma^+$	$3\,^2\Sigma^+$	$1\,^2\Sigma^-$	$2\,^2\Sigma^-$	$1\,^4\Sigma^+$	$2\,^4\Sigma^+$	$1\,^4\Delta$
$c_1\,^4\Sigma^+_{1/2}$	2.8			74.1							23.8						
	3.0			95.7		1.2					1.9						
	3.5			1.9	8.0			1.8			83.5		4.1				
	3.8				46.8						3.7		1.3		44.5		
	4.0														96.6		
	4.1														96.5		
	4.25			15.7						1.4					80.5		
	4.4				1.8		1.2			4.3		3.5	87.7				
	5.0						9.5		6.5		77.8						3.9
	5.5						61.3	32.0			1.7						3.4
	6.0						6.6									92.2	
	6.5			4.8	2.4		21.1	7.3			3.0	1.1	4.2				53.8
$^2\Pi_{1/2}$	2.8			23.2								76.0					
	3.0				98.5												
	3.5				88.6						9.0						
	4.0				79.0						2.2		2.2				13.2
	4.25			3.7	20.6												74.3
	4.6			12.9	2.5												82.9
	5.0						61.3	1.4			5.4	5.8	17.4				5.8
	5.5				2.7		43.5										50.5
	7.0						71.3	15.6			5.1						5.4

[a]The most important configurations and some of the corresponding λ–s states in the Franck–Condon region are $\sigma^2\pi^4\pi^*$ ($1\,^2\Pi$), $\sigma^2\pi^3\pi^{*2}$ (2,3,4 $^2\Pi$, $1\,^4\Pi$), $\sigma^2\pi^4\sigma^*$ ($1\,^2\Sigma^+$), $\sigma\pi^4\pi^{*2}$ ($2\,^2\Sigma^+$, $1\,^2\Sigma^-$, $1\,^2\Delta$, $1\,^4\Sigma^-$), $\sigma^2\pi^3\pi^*\sigma^*$ ($2\,^2\Sigma^-$, $2\,^2\Delta$, $1\,^4\Sigma^+$, $1\,^4\Delta$, $2\,^4\Sigma^-$), and $\sigma\pi^4\pi^*\sigma^*$ ($2\,^4\Pi$). Entries are only made for contributions with $c^2 \geqslant 1.0\%$.

denoted A_i, $i=1$–4 and G, H, respectively. In addition, it was initially thought[15] that the A excited states of BiO originate primarily from $2\,^2\Pi$ rather than $^4\Pi$ until calculations[7] showed that this was not the case.

The next lowest states in the SbO spectrum come from the $\sigma\rightarrow\pi^*$ $^4\Sigma^-$ states, denoted as b_1 and b_2, respectively. These states were not known experimentally at the time that the present calculations were carried out. As with the A state below, however, it can be seen that avoided crossings occur for the corresponding adiabatic states at fairly large r values. In Table II one learns that the b_1 (1/2) state starts out as predominantly $^4\Pi$ up to $r=3.0$ a_0 and then changes over to $2\,^2\Pi$ briefly before assuming its $^4\Sigma^-$ composition in the Franck–Condon region of the SbO ground state. At still larger distances, however, it is more properly characterized as $^2\Sigma^+$. The b_2 (3/2) state, by contrast, has very little $^4\Pi$ character even at small r values (Table III). It is of predominantly $2\,^2\Pi$ composition near $r=3.0$ a_0, before changing to $^4\Sigma^-$ in the Franck–Condon region.

The next spectroscopically observed state is the $\pi^*\rightarrow\sigma^*$ $B\,^2\Sigma^+_{1/2}$ (Fig. 2). Inspection of Table II shows that this state alternates in character, assuming at various r values a predominantly $^2\Sigma^-$, $2\,^2\Pi$, $^4\Sigma^+$ or finally $2\,^4\Pi$ composition. It is thus involved in numerous avoided crossings and is influenced by significant nonadiabatic interactions as a result. In the same neighborhood one finds the $\pi\rightarrow\pi^*$ $I\,^2\Phi$ states, which by virtue of their relatively high Ω values (5/2 and 7/2) pass through the dissociation process with very little mixing with other λ-s states. It also needs to be recalled that the $^6\Sigma^+$ and $^6\Pi$ states do not show up in Fig. 2 at all because of the failure to include them in the spin–orbit coupling phase of the calculations.

The C state lies 3200 cm^{-1} above the $B\,^2\Sigma^+_{1/2}$ and has $\sigma\rightarrow\pi^*$ $^2\Sigma^-_{1/2}$ character in the Franck–Condon region. At small r it has a $2\,^2\Pi$ composition (Table II), however, and for $r>4.25$ a_0 it assumes alternately $3\,^2\Pi$, $^4\Sigma^+$, and $^4\Sigma^-$ character before becoming a fairly diffuse mixture of λ-s states beyond $r=5.0$ a_0. The next pair of states are computed to be the $H_1\,^2\Pi_{3/2}$ and $H_2\,^2\Pi_{1/2}$ species. They are best characterized as $3\,^2\Pi$ in the FC region (Tables II–III), but again are seen to be involved in a number of avoided crossings at both shorter and larger r values. For example, H_2 starts out as primarily ($\sigma\rightarrow\pi^*$) $2\,^2\Sigma^+$, while at $r=5.5$ a_0 it is an equal mixture of $^4\Sigma^-$ and $^4\Pi$. The H_1 state lies about 1000 cm^{-1} lower, i.e., the $\Omega=3/2$ component is more stable, consistent with their $\pi^3\pi^{*2}$ electronic configuration near their potential minima. The latter state has a $^2\Delta$ composition at $r=3.0$–3.5 a_0 (Table III) before changing to $3\,^2\Pi$, and by $r=4.6$ a_0 it becomes predominantly $^4\Sigma^+$. It then goes through a $^4\Sigma^-$ phase before changing to a mixture of various λ-s states at $r=6.0$ a_0 and beyond.

The J_1 and J_2 states are dominated by the $\sigma\rightarrow\pi^*$ $^2\Delta$ λ-s species, which at first was thought to be responsible for the C upper state in the experimental interpretation. The $\Omega=5/2$ component (J_1) is computed to lie about 500 cm^{-1} lower than the $\Omega=3/2$ (J_2) near their respective r_e values (Fig. 2). The J_1 state is not able to mix strongly with other $\Omega=5/2$ species, but J_2 is seen from Table III to be predominantly $3\,^2\Pi$ in the $r=3.0$–3.5 a_0 range. Strictly speaking it can only be described as $^2\Delta$ in a narrow range in the neighborhood of $r=3.8$ a_0. At larger bond distances it undergoes numerous avoided crossings, becoming alternately $^4\Sigma^+$, $3\,^2\Pi$, and $2\,^4\Sigma^+$ before degenerating into a relatively diffuse mixture of various λ-s species which is typical for this energy region. Then comes the $c\,^4\Sigma^+$ pair ($\Omega=1/2,3/2$), which are not known experimentally, similarly as the J_1 and J_2 states. The

TABLE III. Composition of the lowest eight $\Omega=3/2$ states of SbO (c^2, %) at various bond distances r (in a_0).[a]

State	r	$1\,^2\Pi$	$2\,^2\Pi$	$3\,^2\Pi$	$4\,^2\Pi$	$1\,^4\Pi$	$2\,^4\Pi$	$1\,^4\Sigma^-$	$2\,^4\Sigma^-$	$1\,^4\Sigma^+$	$2\,^4\Sigma^+$	$1\,^2\Delta$	$2\,^2\Delta$	$1\,^4\Delta$	$2\,^4\Delta$
$X_2\,^2\Pi_{3/2}$	3.0	99.5													
	3.5	99.3													
	4.0	98.8													
	5.0	97.4		1.1											
	6.0	92.1			1.1	5.9									
	7.0	80.5			1.1	17.6									
$a_1\,^4\Pi_{3/2}$	3.0					1.1		98.4							
	3.5		2.1	1.7		95.6									
	4.0		1.8	1.9		95.5									
	5.0	1.0		2.0		96.2									
	6.0	2.0				96.5									
	7.0	1.8				96.8									
$A_1\,^2\Pi_{3/2}$	3.0		3.0	1.5		94.5									
	3.5		58.9					39.4							
	3.9		95.3			2.2		1.5							
	4.0		95.5			2.1		1.3							
	5.0		85.6					1.7		10.6					
	6.0									99.8					
	7.0									99.3					
$b_2\,^4\Sigma^-_{3/2}$	3.0		93.4			3.1						2.7			
	3.5		38.0			1.7		59.7							
	3.7		2.9					95.9							
	4.0		1.3					97.1							
	5.0		11.6	1.7					2.6	83.3					
	6.0		99.5												
	7.0				8.2		14.6					1.0		72.3	
$H_1\,^2\Pi_{3/2}$	3.0		2.4									96.3			
	3.5			7.0	1.3							91.3			
	3.9			91.9		1.7						3.3			
	4.0			91.5		1.7			1.0			2.9			
	4.6		1.5	8.2				1.4	3.9	83.4					
	5.0			5.1				91.0		2.0					
	6.0				10.2		54.5	4.7			17.3			3.7	
	7.0		30.3				5.0		2.5					51.4	6.3
$J_2\,^2\Delta_{3/2}$	3.0			97.7		1.2									
	3.5			90.0		1.3						7.3			
	3.8			3.0	1.0							94.8			
	4.1			1.7					3.2	78.0		16.1			
	4.25			7.6						88.0					
	5.0			62.2		1.9	3.3	5.7	1.7	1.7	6.5	3.5		11.3	
	6.0				1.2		33.7	2.5			60.8				
	7.0		26.2				31.4	10.4						25.1	
$c_2\,^4\Sigma^+_{3/2}$	3.0				94.5				2.3	2.3					
	3.5				18.0				2.8	78.5					
	4.0			2.0					2.9	74.4		20.4			
	4.25				2.7		3.4					92.3			
	4.6			1.8			8.5					87.7			
	5.0			3.0			50.7				2.0	19.7	3.1	17.3	
	6.0				4.0		25.0	26.7						40.4	
	7.0		23.7				30.6	11.0						31.2	
$^4\Delta_{3/2}$	3.0						66.9			24.9				7.5	
	3.5				78.8				3.0	15.9					
	4.0				5.8								1.7	91.1	
	4.4			1.4									2.5	94.1	
	5.0			2.7			17.1				7.7	7.8		60.8	
	6.0													94.0	
	7.0		60.5				30.6							7.7	

[a]The same footnote as in Table II.

$\Omega=1/2$ component (c_1) lies somewhat lower than the $\Omega=3/2$ counterpart. As usual the above λ-*s* designation for these two states is only valid in a fairly narrow range of r values (see Tables II and III). The c_2 state is dominated by the $\sigma\rightarrow\pi^*\,^2\Delta$ λ-*s* state in the $r=4.25$–$4.60\ a_0$ range, for example. The compositions of two other states, denoted $^4\Pi_{1/2}$ and $^4\Delta_{1/2}$, are also listed in Tables II and III, but there does not appear to be any experimental evidence for them at the present time. The next observed state has been denoted $D\,^2\Pi_{1/2}$,[7] suggesting that it might derive from the $\pi\rightarrow\pi^*\ 4\,^2\Pi$ λ-*s* state, but the

TABLE IV. Calculated and experimental spectroscopic properties of SbO (transition energies T_e, bond lengths r_e, and vibrational frequencies ω_e).

	T_e/cm^{-1}		r_e/Å		ω_e/cm^{-1}	
State	Calc.	Expt.	Calc.	Expt.	Calc.	Expt.
$X_1\,^2\Pi_{1/2}$	0	0	1.8364	1.8258[a]	754	816,[a]819[b]
$X_2\,^2\Pi_{3/2}$	2 080	2 272[a,b]	1.8358		751	814[b]
$a_1\,^4\Pi_{3/2}$	14 207	16 862[d]	2.0666		542	558[d]
$a_2\,^4\Pi_{1/2}$	14 390	17 152[d]	2.0673		541	559[d]
$a_3\,^4\Pi_{5/2}$	14 535		2.0678		540	
$a_4\,^4\Pi_{1/2}$	14 802	17 698[d]	2.0652		545	556[d]
$A_1\,^2\Pi_{3/2}$	19 476	20 668,[a]20 794[b]	2.0627		566	569,[a]570[b]
$A_2\,^2\Pi_{1/2}$	20 091	20 801,[a]21 467[b]	2.0702		546	566[b]
$b_1\,^4\Sigma^-_{1/2}$	22 455	24 174[d]	1.9581		632	610[d]
$b_2\,^4\Sigma^-_{3/2}$	22 836		1.9473		611	
$I_1\,^2\Phi_{7/2}$	24 695		2.0750		507	
$I_2\,^2\Phi_{5/2}$	24 863		2.0790		500	
$B\,^2\Sigma^+_{1/2}$	26 616	26 594[a]	1.9418		557	582[a]
$C\,^2\Sigma^-_{1/2}$	29 683	29 747,[a]~29 750[c]	2.0078	1.997[a]	591	571,[a]569[c]
$H_1\,^2\Pi_{3/2}$	30 425	30 315,[a]~30 495[c]	2.0865		495	~546[c]
$H_2\,^2\Pi_{1/2}$	31 371		2.0948		501	
$J_1\,^2\Delta_{3/2}$	32 348		2.0023		681	
$J_2\,^2\Delta_{5/2}$	32 399		1.9944		610	
$c_1\,^4\Sigma^+_{1/2}$	33 192		2.2492		533	
$c_2\,^4\Sigma^+_{3/2}$	34 041		2.1449		856	
$D\,^2\Pi_{1/2}$	⋯	34 544[a]	⋯	2.073[a]	⋯	506[a]

[a]Reference 15.
[b]Reference 16.
[c]Reference 17.
[d]Reference 18.

indication from the present work is that it also probably has a variable composition over the internuclear distance range of spectroscopic interest, and no attempt has been made to characterize it further.

C. Spectroscopic constants

The present computed transition energy T_e, equilibrium bond length r_e, and vibrational frequency ω_e values for the various electronic states of SbO are compared in Table IV with the corresponding experimental data wherever available. The ground state is $X_1\,^2\Pi_{1/2}$ and the calculated r_e value is found to overestimate the corresponding experimental result by 0.0106 Å. The level of agreement is similar to that obtained for antimony fluoride[23] and is notably better than for BiO.[7] Use of the full-core antimony RECP, with consideration of only the $5s$ and $5p$ shells in the CI treatment, thus gives a suitably accurate description of the electronic structure of molecules containing this atom. In BiO it appears essential to employ a semicore RECP, i.e., one in which the penultimate $(5d)$ shell is not described by the effective core potential alone. There also is an indication that the bismuth $5d$ electrons also need to be correlated in the spin–orbit CI to achieve results of comparable accuracy for systems containing this atom.[7] The corresponding X_1 ω_e value for SbO is underestimated in the present calculations by about 60 cm^{-1} (Table IV).

The X_1-X_2 zero-field splitting is computed to be 2080 cm^{-1}, which is 192 cm^{-1} lower than the measured value. The calculations indicate that the X_2 r_e value is 0.0006 Å smaller than that of X_1, but there is as yet no experimental result with which to compare in this case. The calculations also indicate a slightly lower ω_e value for X_2, and this result does have confirmation in the observed data. A more serious deficiency in the theoretical treatment occurs in the determination of the various $a_i\,^4\Pi$ T_e values. The $a_1\,^4\Pi_{3/2}$ is computed to be the most stable of the corresponding Ω multiplets, in agreement with experiment,[18] but its T_e value is calculated to be too low by 2655 cm^{-1}. The corresponding discrepancy in the BiO study is only 1177 cm^{-1}.[7] In general one expects that the correlation energy of the $X\,^2\Pi$ state is significantly greater than that of the $a\,^4\Pi$, with two more open shells, and experience indicates that only the use of a very flexible AO basis set is capable of making up for this difference in a CI treatment. The fact that the SbO $a_i\,^4\Pi$ states are far less mixed with $^2\Pi$ states, as discussed in the preceding section, than are their BiO counterparts probably is a key reason for the occurrence of a smaller T_e underestimation for the heavier of the two oxides. The order of the $a\,^4\Pi$ multiplets is $3/2<1/2<5/2<1/2$, exactly as found for BiO.[7] The energy difference between lowest and highest such multiplet is computed to be only 595 cm^{-1}, also underestimating the observed result of 836 cm^{-1} (Table IV). The location of the $a_3\,^4\Pi_{5/2}$ state is not yet confirmed experimentally, but the computed order has otherwise been demonstrated to be correct. The a_2 and a_4 states with $\Omega=1/2$ each have nearly parallel potential energy curves, as can be judged from Fig. 3, in which all states of this Ω value are considered. No r_e determinations have yet been made experimentally for any of the $^4\Pi$ states, but the corresponding vibrational frequencies have recently been observed to fall in the 556–559 cm^{-1} range,[18] only 10–15 cm^{-1} greater than computed in the present work (Table IV).

The $A\,^2\Pi$ state is found to be inverted, consistent with observation.[16] The zero-field splitting is computed to be 615 cm^{-1}, in good agreement with the observed result of 673 cm^{-1} of Balfour and Ram.[16] An earlier value of 133 cm^{-1} (with the opposite order of the two spin components)[9,15] seems therefore to be erroneous. The computed r_e values for both A_1 and A_2 are similar to those found for the $a\,^4\Pi$ states, consistent with their equivalent electronic configurations, and all these values are 0.23 Å larger than for the X_1 and X_2 systems. The A_1 and A_2 ω_e values are known experimentally,[15,16] and our present results agree within 20 cm^{-1} in each case. Both these states undergo avoided crossings near $r=5.0$ a_0 which lead to relatively large recombination barriers (Figs. 3 and 4).

The next pair of states appears to be the $b_1\,^4\Sigma^-_{1/2}$ and $b_2\,^4\Sigma^-_{3/2}$, with computed T_e values of 22 455 and 22 836 cm^{-1} (Table IV). Recent experiments[18] have located the b_1 state 1719 cm^{-1} higher than has been computed. The theoretical underestimation is only slightly worse than for the $A\,^2\Pi$ states, and significantly better than for the corresponding $a\,^4\Pi$ states. The $^4\Sigma^-$ splitting does not occur internally, unlike the case for the $a\,^4\Pi$ states, and thus arises because of unequal perturbations from other neighboring λ-s states. There is unfortunately as yet no experimental verification that the $\Omega=3/2$ component is the higher-lying of these two states. The two computed r_e values differ by 0.01 Å from each other (Table IV), but are both more than 0.1 Å smaller

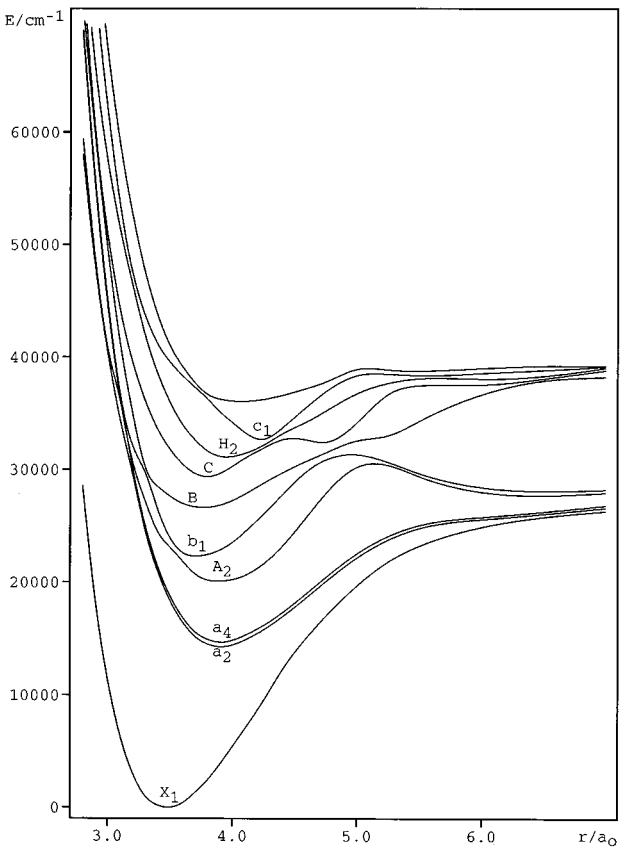

FIG. 3. Computed potential energy curves for the lowest-lying $\Omega=1/2$ states of the SbO molecule.

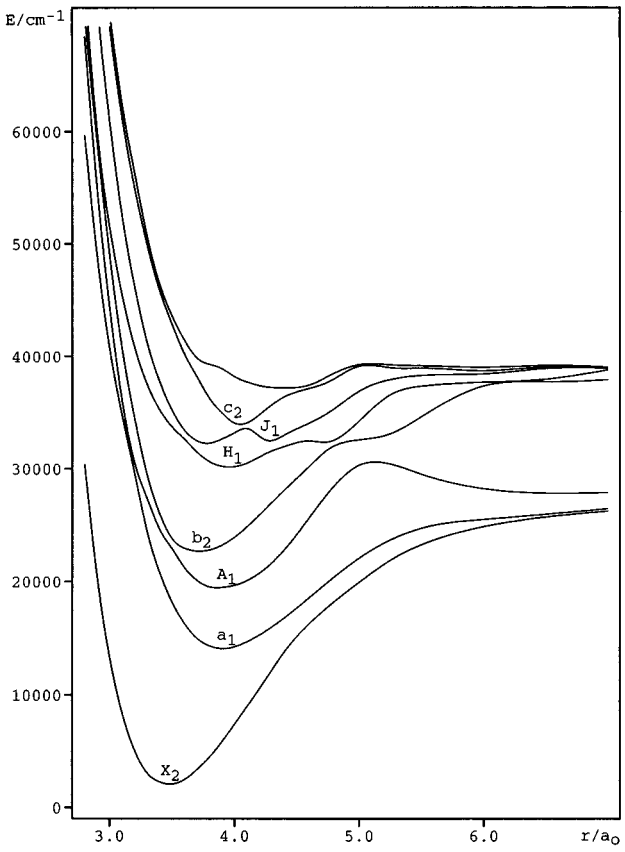

FIG. 4. Computed potential energy curves for the lowest-lying $\Omega=3/2$ states of the SbO molecule.

than any of the $a\ ^4\Pi$ and $A\ ^2\Pi$ results. Since these two groups of states differ primarily in their respective occupation of the σ and π bonding orbitals, the indication is that the origin for this large distinction should be sought in the AO composition of these two MO's (see the discussion in Sec. III A). The b ω_e values are computed to be somewhat higher than those of the $A\ ^2\Pi$ and $a\ ^4\Pi$ states, consistent with the r_e findings, but no experimental results are as yet available to check this point. Because of their bond length differences, the b_1 and A_2 states undergo an avoided crossing near $r=3.6$ a_0 (Fig. 3). A similar feature occurs for their $\Omega=3/2$ counterparts, b_2 and A_1 (Fig. 4).

The next lowest T_e values according to the calculations are those of the $I_1\ ^2\Phi_{5/2}$ and $I_2\ ^2\Phi_{7/2}$ states. Their potential curves are shown in Fig. 5 for comparison with the other computed $\Omega=5/2$ states, a_3 and J_1. There is only a small splitting of 168 cm^{-1} computed for the two $^2\Phi$ Ω components. The corresponding r_e values differ by 0.0040 Å and are somewhat greater than those of the lower-lying $\pi\rightarrow\pi^*$ states. The ω_e values are also smaller than for these states.

The $B\ ^2\Sigma^+$ state has only one component ($\Omega=1/2$). The present calculated T_e value is in very good agreement with experiment,[12] while the ω_e value is underestimated by 25 cm^{-1}.[16] Based on the computed r_e value it appears that the σ^* orbital strongly occupied in this state is notably more antibonding than the π^* (occupied instead in $X\ ^2\Pi$). In BiO the analogous state is referred to as K.[7] The potential curves of Fig. 3 indicate that the b_1 and B states also undergo an avoided crossing at relatively short bond distances, and so significant nonadiabatic effects are expected in the corresponding energy region. The $C\ ^2\Sigma^-$ state also has only a single ($\Omega=1/2$) component. Again in this case there is very good agreement between computed and measured T_e values (Table IV). As a result of the work of Balfour and Ram[17] the assignment for this state was changed from $^2\Delta$ to $^2\Sigma^-$, and the present calculations support this decision. Its r_e value is overestimated by only 0.011 Å in the present study. The computed result exceeds that of $^4\Sigma^-$, which arises from the same $\sigma\rightarrow\pi^*$ excitation, by 0.05 Å and the corresponding ω_e value overestimates the observed data[15,16] by 20 cm^{-1}, instead of the more common underestimation usually found in other comparisons already discussed. The fact that the C state undergoes an avoided crossing with the next higher $\Omega=1/2$ species at slightly larger bond distances than r_e is likely responsible for both of these irregularities.

The upper state in question is the $H_2\ ^2\Pi_{1/2}$ which originates from the $\pi\rightarrow\pi^*$ excitation, hence with a somewhat larger bond length than for the $\sigma\rightarrow\pi^*$ $C\ ^2\Sigma^-$ state. This $^2\Pi$ is also inverted, with the $\Omega=3/2$ component (H_1) computed to lie 946 cm^{-1} lower. Experimentally only H_1 has been detected and there is again very good agreement between calculation and experiment with regard to its T_e value (Table IV). No r_e value has been reported but the observed ω_e result is 51 cm^{-1} higher than calculated, consistent with the general

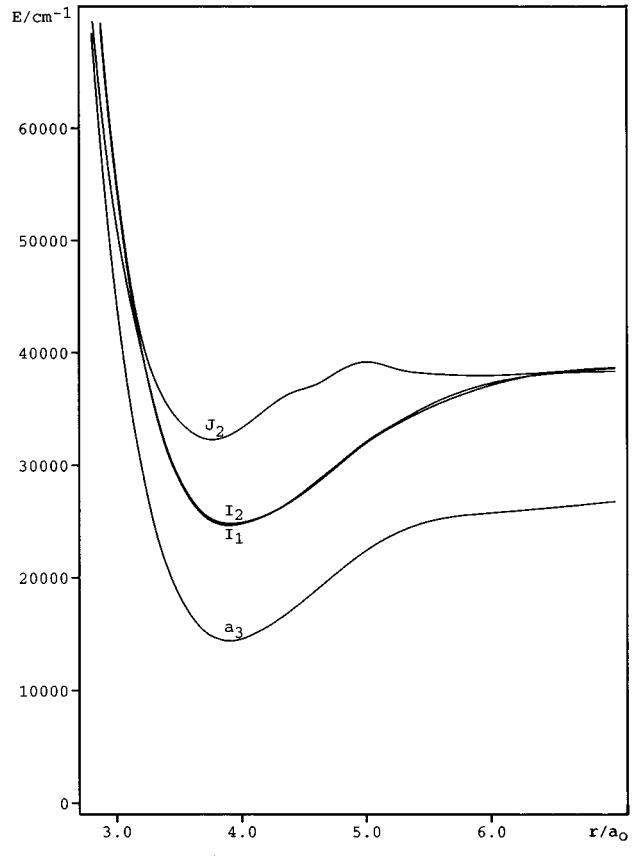

FIG. 5. Computed potential energy curves for the lowest-lying $\Omega=5/2$ (a_3, I_1, and J_1) and $\Omega=7/2$ (I_2) states of the SbO molecule.

trend noted earlier for many other states. The computed r_e value is quite similar in magnitude to that found for the other $\pi\rightarrow\pi^*$ states. It should be noted that the H_1 $\Omega=3/2$ state does not undergo a similar avoided crossing as H_2 (Fig. 4) with lower-lying states. Inevitably, however, other avoided crossing do occur with higher-lying states.

The $^2\Delta$ pair of Ω states once thought to be responsible for the C state observation[10,15] are computed to have T_e values of 32 348 and 32 399 cm^{-1} and are denoted $J_1\,^2\Delta_{3/2}$ and $J_2\,^2\Delta_{5/2}$, respectively. The J_1 species undergoes an avoided crossing with the $H_1\,^2\Pi_{3/2}$ state (Fig. 4) which produces a slight increase in its r_e value relative to J_2 as well as an increased ω_e value. The latter state also shows a maximum in the neighborhood of $r=5.0\ a_0$ (Fig. 5). The c_1 and c_2 states have not been observed experimentally as yet. There is also a large difference in their respective r_e and ω_e values, which again is caused primarily by the avoided crossing between the $\Omega=3/2$ states (Fig. 4). The T_e value for c_2 is 849 cm^{-1} higher than for c_1 (Table IV). In view of the high density of states in this energy region, it seemed best to end the present study at this point. A $D\,^2\Pi_{1/2}$ state has been reported[15] with a T_e value in this range (34 544 cm^{-1}), but it is difficult to say what the actual composition of such an upper state may be, although it can be expected that the $\pi\rightarrow\pi^*$ $4\,^2\Pi$ should play an important role at some r values. For completeness we have summarized the compositions of the next two quartet-dominated states, $^4\Pi_{1/2}$ and $^4\Delta_{3/2}$, in Tables II and III, respectively. Huber and Herzberg[15] also give some spectroscopic constants for E, F, and G states which are thought to lie somewhat higher in the spectrum.

Finally, the calculations indicate that the ground state D_e value lies in the 28 000–29 000 cm^{-1} range (Fig. 2), i.e., 3.5–3.6 eV. One expects this result to be an underestimate because a multiple bond is present in the equilibrium structure and no bond functions have been added to the present AO basis. Based on the observed predissociation of low rotational levels of the $v=2$ vibrational state of $D\,^2\Pi_{1/2}$, Rai *et al.*[28] concluded that the D_0 value for the $X\,^2\Pi_{1/2}$ ground state should be less than or equal to the corresponding measured energy separation of 4.29 eV (34 574 cm^{-1}); an upper limit of 4.39 eV is given in Ref. 15 for the same quantity. The present calculations show that the most likely candidate to cause the $D\,^2\Pi_{1/2}$ ($4\,^2\Pi$) predissociation in the required energy range is the $^4\Sigma^+$ state (Fig. 1). Note that the latter eventually dissociates into the lowest atomic limit, as suggested by Rai *et al.*[28] The clear indication from the present results is that the 4.29 eV value mentioned above represents a considerable overestimate of the true D_0 quantity, however, and especially that the present calculated value of 3.5–3.6 eV is probably accurate to within a few tenths of an eV based on the potential curves in Fig. 1.

IV. COMPUTED EINSTEIN COEFFICIENTS AND RADIATIVE LIFETIMES

The CI wave functions discussed above have also been employed to compute electronic and vibrational transition moments and corresponding Einstein coefficients for spontaneous radiative emission. In later work we will compare these results for various arrays of vibrational transitions in band systems of SbO and BiO.[7] In this study emphasis will be placed on the radiative lifetimes of the $v'=0$ levels of the various SbO excited electronic states, which are calculated by summing over the Einstein coefficients with all lower-lying vibrational states and inverting. The results are given separately for transitions into $X_1\,^2\Pi_{1/2}$ and $X_2\,^2\Pi_{3/2}$ in Table V, and these are combined for comparison with available experimental data.[18] The X_2 state itself is found to have a relatively long lifetime of 0.29 s based on X_2-X_1 transitions. Such a result is very difficult to verify experimentally and no such observed result has yet been reported. In BiO a measured value of 0.48 ms has been obtained by Fink *et al.*,[18] and this distinction gives a clear idea of the different effects of spin–orbit coupling between these two group VA oxides.

The computed radiative lifetimes for the $a\,^4\Pi$ states of SbO fall in the 0.3–16.0 ms range. The $a_2\,^4\Pi_{1/2}$ state has a relatively strong parallel transition to X_1 and its lifetime is calculated to be only 0.353 ms. This result is consistent with the experimental findings, since this is the only one of the $a\,^4\Pi$ species for which a lifetime could be determined to date.[18] The value reported is 0.190 ms, in moderately good agreement with the calculated value. The $3\,^2\Pi$ admixture to the $a_2\,^4\Pi_{1/2}$ state (Table II) seems to be primarily responsible for the relatively high intensity of the a_2-X_1 transition.

The $A_i\,^2\Pi$ states have fairly large Einstein coefficients by virtue of parallel transitions to $X\,^2\Pi$. Calculated $v'=0$ lifetimes of 17.7 and 11.5 μs for A_1 and A_2, respectively,

TABLE V. Radiative lifetimes of excited states of SbO ($v'=0$); calculated partial lifetimes τ_1 and τ_2 for transitions to $X_1\,^2\Pi_{1/2}$ and $X_2\,^2\Pi_{3/2}$, respectively, as well as calculated and experimental total lifetime τ.

State	Calculated			Experiment[a]
	τ_1/s	τ_2/s	τ/s	τ/s
$X_2\,^2\Pi_{3/2}$	0.29		0.29	
$a_1\,^4\Pi_{3/2}$	6.4×10^{-3}	4.7×10^{-3}	2.7×10^{-3}	
$a_2\,^4\Pi_{1/2}$	356×10^{-6}	37.6×10^{-3}	353×10^{-6}	190×10^{-6}
$a_3\,^4\Pi_{5/2}$		5.4×10^{-3}	5.4×10^{-3}	
$a_4\,^4\Pi_{1/2}$	5.0×10^{-3}	10.0×10^{-3}	3.3×10^{-3}	
$A_1\,^2\Pi_{3/2}$	1.8×10^{-3}	17.9×10^{-6}	17.7×10^{-6}	20×10^{-6}
$A_2\,^2\Pi_{1/2}$	11.6×10^{-6}	1.4×10^{-3}	11.5×10^{-6}	13×10^{-6}
$b_1\,^4\Sigma^-_{1/2}$	63.9×10^{-6}	352×10^{-6}	54×10^{-6}	$\geqslant 20\times10^{-6}$
$b_2\,^4\Sigma^-_{3/2}$	0.27	144×10^{-6}	144×10^{-6}	
$B\,^2\Sigma^+_{1/2}$	1.25×10^{-6}	1.9×10^{-6}	0.75×10^{-6}	3.0×10^{-6}
$C\,^2\Sigma^-_{1/2}$	0.60×10^{-6}	1.9×10^{-6}	0.45×10^{-6}	0.45×10^{-6}
$H_1\,^2\Pi_{3/2}$	12.7×10^{-6}	3.0×10^{-6}	2.4×10^{-6}	
$H_2\,^2\Pi_{1/2}$	31.3×10^{-6}	80.7×10^{-6}	22.6×10^{-6}	

[a]Reference 18.

compare well with recent observed results of 20 and 13 μs, respectively.[18] These states are most comparable to the G and H species of BiO,[7] whose computed and observed lifetimes are of similar magnitude to their SbO counterparts. This result suggests that spin–orbit coupling plays a fairly minor role in these effects, as one would expect since mainly $^2\Pi$–$^2\Pi$ transitions are involved. The next low-lying states, $b_1\,^4\Sigma^-_{1/2}$ and $b_2\,^4\Sigma^-_{3/2}$, have longer lifetimes than either A_1 or A_2 but significantly shorter than the $a\,^4\Pi$ states. The fact that parallel transitions to $X\,^2\Pi$ dominate in the associated intensity pattern underscores the fact that the $^4\Sigma^-$ character itself plays a minor role in these results, however, but rather other admixed λ-s states (see Tables II and III). Experimentally,[18] a lower limit has been found for the b_1 state of 20 μs, compared to the calculated value of 54 μs. It should also be noted that $^4\Sigma^-$–$a\,^4\Pi$ transitions are fairly strong as well and when their Einstein coefficients are included, a lifetime of 12.8 μs results. No comparable value has yet been reported for $b_2\,^4\Sigma^-_{3/2}$, which is at least consistent with the computations since they find that its radiative lifetime is nearly three times longer than that of b_1. When b_2–$a\,^4\Pi$ transitions are included, the computed lifetime decreases to 16.7 μs, however. Thus the indication is that this transition should be monitored rather than either the b_2–X_1 or b_2–X_2 species in order to have the best opportunity to measure the lifetime of the b_2 upper state.

The $B\,^2\Sigma^+_{1/2}$ is one of the shortest-lived species in the SbO spectrum according to the present calculations. The computed value of 0.75 μs is four times shorter than the corresponding measured result, a fairly large discrepancy considering the magnitude of the intensities involved. Both parallel and perpendicular transitions contribute significantly to this result. One possible cause for this discrepancy may be nonadiabatic effects arising from overlap with the lower-energy $b_1\,^4\Sigma^-_{1/2}$ state (Fig. 3). In Ref. 1 there is already some indication of such an effect, for example. Since b_1–X transitions are notably weaker than B–X, it follows that strong nonadiabatic mixing between these upper states would tend to remove intensity from the latter transitions. Consistent with this possibility is the computed finding that the $v'=7$ and 8 lifetimes of the b_1 state are only about half as long as $v'=0$. In general, one must expect that purely adiabatic calculations of such quantities become less reliable as the density of states increases for higher energy species.

The $C\,^2\Sigma^-_{1/2}$ state possesses an even shorter lifetime of 0.45 μs according to the calculations. This result is in very good agreement with the measurements of Fink *et al.*[18] In this case there is no avoided crossing that seems likely to affect the $v'=0$ vibrational level (Fig. 3). The last results listed in Table V are for the $H_1\,^2\Pi_{3/2}$ and $H_2\,^2\Pi_{1/2}$ states. Again parallel transitions to X_1 and X_2, respectively, provide the largest contributions to these Einstein coefficients. Values of 2.4 ($\Omega=3/2$) and 22.6 μs ($\Omega=1/2$) have been computed in the present study for these two states. This result is at least consistent with the available measurements[18] since the H_1–X_2 transition has been identified in the spectrum, while H_2–X_1 has not, but no quantitative value for the lifetime of either of the H states has yet been reported experimentally.

V. CONCLUSION

Relativistic effective core potentials have been employed in a spin–orbit CI treatment to compute potential energy surfaces and Einstein coefficients for transitions between various pairs of vibrational states. The identities of the $X\,^2\Pi$, $A\,^2\Pi$, $B\,^2\Sigma^+$, $C\,^2\Sigma^-$, and $H\,^2\Pi$ states have been confirmed on this basis and accurate values of spin–orbit splitting, T_e, r_e, and ω_e values have been obtained in each case. It has also been possible to characterize the various $a\,^4\Pi$ and $b\,^4\Sigma^-$ states lying in the same energy region, thereby aiding in the experimental identification[18] of three of the four multiplets of the former λ-s species and the $\Omega=1/2$ component of the latter. The computed r_e values underscore a clear difference in the bonding strengths of the σ and π MO's in SbO, as well as in the antibonding character of σ^* and π^*. Such distinctions are found to be much more pronounced in this system than in its heavier isovalent counterpart, BiO,[7] and this relationship can be understood on the basis of the different electronegativities of the Sb und Bi atoms.

The computed SbO λ-s curves exhibit very few avoided crossings in the ground-state Franck–Condon region up to $r=5.0\ a_0$, at which point the $^{2,4}\Sigma^+$ and $^{2,4}\Pi$ species correlating with the five-open-shell atomic limits, Sb $(^4S_u)+O(^3P_g)$, begin to interact strongly with the configurations possessing only one or three open shells which dominate at smaller bond distances. Inclusion of the spin–orbit interaction leads to numerous weakly avoided crossings, but the resulting nonadiabatic effects are much less important than in BiO. In particular, the $a_1\ ^4\Pi_{3/2}$ state does not interact nearly as strongly with $X_2\ ^2\Pi_{3/2}$ in antimony oxide. The calculations have also found the I_1 and $I_2\ ^2\Phi$ states originating from a $\pi\rightarrow\pi^*$ excitation to have T_e values in the 25 000 cm^{-1} region. This finding has not yet been verified experimentally, presumably because the high Ω values of the $^2\Phi$ species cause transitions to the $X\ ^2\Pi$ states to be quite weak. The $\sigma\rightarrow\pi^*\ J\ ^2\Delta$ states are placed near 32 000 cm^{-1}, slightly above the $H\ ^2\Pi$ states, but just below the $c\ ^4\Sigma^+$ species.

Finally, the radiative lifetimes of the $v'=0$ levels of each of the SbO electronic states have been calculated from Einstein spontaneous emission coefficients. Comparison with recent experimental values[18] indicates that such quantities can generally be predicted within a factor of 2 at the present level of treatment, at least for values in the μs range. Six such comparisons have been possible to date. The X_2-X_1 transition is found to be especially weak in this system, corresponding to an X_2 lifetime of 0.29 s, but no experimental verification has yet been possible in this case. The discrepancy in the computed $B\ ^2\Sigma^+_{1/2}$ lifetime is somewhat larger than usual and it is suggested that this result might be related to a nonadiabatic interaction between it and the lower-lying $b_1\ ^4\Sigma^-_{1/2}$ state. Overlapping bands between these two sets of vibrational levels had been assumed earlier by Rai and Rai,[1] consistent with the above interpretation. For this reason it would be interesting to measure the lifetimes of a series of b_1 and B vibrational levels to see if they deviate significantly from their $v'=0$ counterparts, especially in the energy region in which an avoided crossing between their respective potential curves is found.

In general, a very good description of the SbO spectrum is obtained on the basis of the present spin–orbit CI treatment employing full-core RECP's and only eleven electrons in the active space for the calculations. The situation is not nearly so simple for bismuth oxide, however, in which case the bismuth $5d$ subshell is best treated without the benefit of core potentials and there is an indication that these electrons should also be included in the active space of the CI treatment. More calculations are in progress for other members of this series of molecules, such as AsO, SbS, and BiS.

ACKNOWLEDGMENTS

The authors are very grateful for numerous discussions with Professor E. H. Fink and Dr. O. D. Shestakov during the course of the present study. Special thanks are also due to Professor R. M. Pitzer for making available his ECP spin–orbit integral program to us. This work was supported in part by the Deutsche Forschungsgemeinschaft in the form of a Forschergruppe grant. The financial support of the Fonds der Chemischen Industrie is also hereby gratefully acknowledged. One of us (A.B.A.) thanks the Alexander von Humboldt Foundation for the granting of a stipend.

[1] S. B. Rai and D. K. Rai, Chem. Rev. **84**, 73 (1984).
[2] Y. S. Lee, W. C. Ermler, and K. S. Pitzer, J. Chem. Phys. **67**, 5861 (1977).
[3] P. A. Christiansen, Y. S. Lee, and K. S. Pitzer, J. Chem. Phys. **71**, 4445 (1979).
[4] W. C. Ermler, Y. S. Lee, P. A. Christiansen, and K. S. Pitzer, Chem. Phys. Lett. **81**, 70 (1981).
[5] P. A. Christiansen, K. Balasubramanian, and K. S. Pitzer, J. Chem. Phys. **78**, 5087 (1982).
[6] A. B. Alekseyev, H.-P. Liebermann, I. Boustani, G. Hirsch, and R. J. Buenker, Chem. Phys. **173**, 333 (1993).
[7] A. B. Alekseyev, H.-P. Liebermann, R. J. Buenker, G. Hirsch, and Y. Li, J. Chem. Phys. **100**, 8956 (1994).
[8] B. C. Mukherjee, Z. Phys. **70**, 552 (1931).
[9] A. K. Sengupta, Ind. J. Phys. **13**, 145 (1939); **17**, 216 (1943).
[10] S. V. J. Lakshman, Z. Phys. **158**, 367 (1960); **158**, 386 (1960).
[11] M. Shimauchi, Sci. Light **9**, 109 (1960).
[12] D. V. K. Rao and P. T. Rao, Curr. Sci. **37**, 310 (1968).
[13] B. Rai, K. N. Upadhya, and D. K. Rai, J. Phys. B **3**, 1374 (1970).
[14] S. B. Rai, B. Rai, and D. K. Rai, Can. J. Phys. **52**, 592 (1974).
[15] K. P. Huber and G. Herzberg, *Molecular Spectra and Molecular Structure* (Van Nostrand Reinhold, Princeton, 1979), Vol. 4.
[16] W. J. Balfour and R. S. Ram, J. Mol. Spectrosc. **105**, 246 (1984).
[17] W. J. Balfour and R. S. Ram, J. Mol. Spectrosc. **130**, 382 (1988).
[18] E. H. Fink and O. D. Shestakov (private communication).
[19] R. B. Ross, J. M. Powers, T. Atashroo, W. C. Ermler, L. A. LaJohn, and P. A. Christiansen, J. Chem. Phys. **93**, 6654 (1990).
[20] I. Boustani, S. N. Rai, H.-P. Liebermann, A. B. Alekseyev, G. Hirsch, and R. J. Buenker, Chem. Phys. **177**, 45 (1993).
[21] L. F. Pacios and P. A. Christiansen, J. Chem. Phys. **82**, 2664 (1985).
[22] W. H. E. Schwarz and R. J. Buenker, Chem. Phys. **13**, 153 (1976).
[23] R. J. Buenker and S. D. Peyerimhoff, Theor. Chim. Acta **35**, 33 (1974); **39**, 217 (1975); R. J. Buenker, S. D. Peyerimhoff, and W. Butscher, Mol. Phys. **35**, 771 (1978).
[24] R. J. Buenker and R. A. Philips, J. Mol. Struct. Theochem. **123**, 291 (1985).
[25] E. R. Davidson, in *The World of Quantum Chemistry*, edited by R. Daudel and B. Pullman (Reidel, Dordrecht, 1974), p. 17.
[26] G. Hirsch, P. J. Bruna, S. D. Peyerimhoff, and R. J. Buenker, Chem. Phys. Lett. **52**, 442 (1977); D. B. Knowles, J. R. Alvarez-Collado, G. Hirsch, and R. J. Buenker, J. Chem. Phys. **92**, 585 (1990).
[27] J. W. Cooley, Math. Comput. **15**, 363 (1961).
[28] B. Rai, K. N. Upadhya, and D. K. Rai, J. Phys. B **3**, 1374 (1970).